Chem. Res. Chinese Universities, 2020, 36(4), 690—693 doi: 10.1007/s40242-020-0198-8

Article

Operando Observation of Structural Evolution and Kinetics of $Li[Ni_{0.6}Co_{0.2}Mn_{0.2}]O_2$ at Elevated Temperature

ZHANG Guobin[1,2#], PAN Xuelei[1#], YU Kesong[1#], YAN Mengyu[1*], XIONG Fangyu[1], WU Liming[1], DENG Xuanwei[1], ZHANG Haining[1] and MAI Liqiang[1,3*]

1. State Key Laboratory of Advanced Technology for Materials Synthesis and Processing, Wuhan University of Technology, Wuhan 430070, P. R. China;

2. Department of Mechanical Engineering, City University of Hong Kong, Hong Kong 999077, P. R. China;

3. Foshan Xianhu Laboratory of the Advanced Energy Science and Technology Guangdong Laboratory, Xianhu Hydrogen Valley, Foshan 528200, P. R. China

Abstract $Li[Ni_{0.6}Co_{0.2}Mn_{0.2}]O_2$(NCM622) is one of the best commercialized cathodes in the battery field. However, poor cyclability at relatively high temperature hinders its multiple usages. Here, *operando* tests were performed to investigate the phase transitions and electron/ion transfer process of layered NCM622 at 25 and 55 °C. The identified spinel structure resulting in the poor cyclability at 55 °C guides the commercialization of batteries at high temperature.

Keywords Lithium-ion battery; NCM622; High temperature; *In situ* X-ray diffraction(XRD)

1 Introduction

With the increasing awareness of environmental concerns, clean and renewable energy has become the mainstream[1,2]. In the future, advanced batteries, as one of the best candidates, play an important role in electronics, vehicles, and electricity grids, etc.[3]. Especially in recent years, the advances in lithium-ion batteries(LIBs) have enabled a rapid growth of hybrid-electric vehicles(HEVs) and electric vehicles(EVs), such as Nissan Leaf, and will reshape the future personal transportation. However, the key, to fully replace the gasoline-powered automobiles by HEVs and EVs, lies on the increscent of the energy density and the reduction of the cost of LIBs. This highly depends on the safe and low-cost cathode materials with high energy and power capability. A promising cathode material is the Ni-rich layered lithium transition metal oxides, $LiNi_{1-x-y}Co_xMn_yO_2$(NCM, $x+y\leqslant 0.5$), which can reversibly deliver a high specific capacity beyond 140 mA·h/g at a high operating voltage >3.8 V[4].

Increasing the Ni content in NCM will improve the lithium utilization at selected voltage window, thereby will improve the specific capacity, however, shorten its cycle life. The fast capacity fading in Ni-rich NCM is commonly attributed to their interfacial or structural instability at high delithiation degrees, which reduces the cycling life of the cell[5]. The structure instability is mainly originated from the high reactivity of Ni^{4+} and active migration of Ni^{2+} in the highly delithiated NCM. The former will result in serious side reactions between charged cathode and the electrolytes[6]. Meanwhile, the thermodynamic instability of high delithiated NCM, mainly aroused from the unstabilized interlayer oxygen-oxygen interaction, drives the migration of transition metal ions(mainly Ni^{2+}) into the empty Li layer to stabilize the structure, accompanied by the oxygen release and vacancy formation[7]. In particular, the H2-H3 transition occurring at high delithiation degrees, as observed for $LiNiO_2$[8] and Ni-rich NCM[9], introduces abrupt and anisotropic volume changes and thus larger internal stresses, which will damage the cathode. These irreversible processes not only introduce resistive layers[cathode electrolyte interphase(CEI) and defect spinel][10], but also cause metal dissolution(mainly Ni), consuming active materials and poisoning the anode. All these factors contribute together to the rapid impedance build-up, voltage decay, and capacity fading of Ni-rich NCM.

The phase evolution processes have been mostly investigated microscopically, primarily by the electron microscope[11], X-ray absorption fine structure spectroscopy[12] or time-of-flight secondary-ion mass spectrometry[13]. These spatially resolved microscopic studies, however, did not investigate the electrochemical properties of the intermediate phases[14], which could be due to the insufficient instrumental capability, insufficiently cycled cells or temperature customized *in situ* cells[2].

*Corresponding authors. Email: mlq518@whut.edu.cn; ymymiles@whut.edu.cn

# These authors contributed equally to this work.

Received June 20, 2020; accepted July 17, 2020.

Supported by the Project of the Foshan Xianhu Laboratory of the Advanced Energy Science and Technology Guangdong Laboratory, China(No.XHT2020-003), the National Natural Science Foundation of China(No.51521001), the National Key Research and Development Program of China(No.2016YFA0202603) and the Fundamental Research Funds for the Central Universities of China(No.WUT: 205201019).

Herein, systematic cyclic voltammetric method and *in situ* X-ray diffraction(XRD) study of layered $Li[Ni_{0.6}Co_{0.2}Mn_{0.2}]O_2$ (NCM622), were performed to probe the electrochemical property and structural evolution. The layered-to-spinel phase transition was clearly observed *via in situ* XRD for NCM622 cycled at 55 °C. The formation of the spinel phase is presumably due to its thermodynamic stability at highly delithiated state during elevated temperatures.

2 Experimental

Firstly, to characterize the structure, *Rietveld* refinement was employed as shown in Fig.1(A). The result shows the NCM622 with lattice parameters of a=0.2869 nm and c=1.4229 nm and the Li/Ni mixing ratio is 2.0%. Also the high intensity ratios of (003) and (104) peaks(I_{003}/I_{104}: *ca*. 2.0) and well splitting of (108)/(110) peaks indicate the layered feature (Fig.S1, see the Electronic Supplementary Material of this paper). The energy dispersive spectrum and the elemental mapping results demonstrate the uniform distribution of Ni, Co and Mn elements with a ratio of nearly 3:1:1[Table 1 and Fig.1(B)—(E)]. As for the morphology, the material presents layered secondary particles with sizes of *ca*. 15 μm that are composed of primary particles with sizes of hundreds of nanometers depicted in Fig.S2(see the Electronic Supplementary Material of this paper). All these imply the high quality of the pristine materials so no other factors could influence the materials performance.

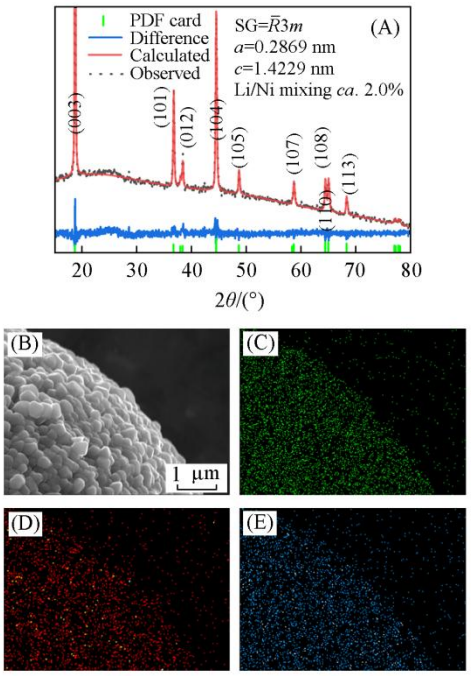

Fig.1 XRD patterns of NCM622(A), the scanning electron microscope images of pristine NCM622(B) and the energy dispersive spectra of Ni(C), Co(D) and Mn(E)

(A) The lattice parameters and Li/Ni mixing degree were calculated from the *Rietveld* refinement.

At 25 °C, when cycled up to 4.2 V, NCM622 shows an initial charge capacity of *ca*.160 mA·h/g and a discharge capacity of *ca*.127 mA·h/g, with a Coulombic efficiency of *ca*. 80.06% at 0.3 C(1C=180 mA/g for NCM622), which is compatible with that of the Ni-rich NCM[15]. At 55 °C within 3.0—4.2 V, it delivers higher initial charge and discharge capacities of *ca*.170 and *ca*.146 mA·h/g with a Coulombic inefficiency of *ca*. 14.29% at 0.3 C(Fig.S3, see the Electronic Supplementary Material of this paper). Also, as for the cyclic voltammetry(CV) curves at 0.03 mV/s, one pair of obvious peaks were found to be located at 3.74 and then 3.82 V at 25 °C for the first and second cycles, where 3.78 and 3.87 V for 55 °C (Fig.S4, see the Electronic Supplementary Material of this paper). The plateau can be assigned to the structural transitions from hexagonal phase 1(H1) to monoclinic phase(M) at *ca*. 3.7 V(so called H1-M transition) as suggested for $LiNiO_2$[8,9].

Table 1 Element atomic fraction of Mn, Co and Ni

Element	Atomic fraction(%)
Mn	0.73
Co	0.73
Ni	1.98

3 Results and Discussion

To illuminate the charge storage mechanism of layered NCM622 at the elevated temperature, the CVs at different scan rates(0.1, 0.2, 0.4, 0.6 and 0.8 mV/s) were employed[Fig.2(A) and (B)]. Only one pair of redox peaks can be observed in the CV curves at both 25 and 55 °C. As the scan rate increases, the cathodic peaks show a nearly linearly shift to higher potential/current at 25 and 55 °C, where 0.8 mV/s at 25 °C is an exception, which may be due to the sluggish ion diffusion at 25 °C. According to Dunn and co-workers[16], the diffusion controlled contribution($k_2v^{1/2}$) and capacitive(k_1v) contribution can be distinguished *via* the following equation[Eq.(1)]:

$$i_p = k_1v + k_2v^{1/2} \quad (1)$$

where i_p is the peak current, v is the scan rate, thus the transfer kinetics is concluded the i_p *versus* $v^{1/2}$ plot. The fitted plot shows that the i_p has nearly linear relationship with the $v^{1/2}$ shown in Fig.2(C) and (D), the fitted intercept and slop at 25 and 55 °C from anodic and cathodic peaks are shown in Table S1(see the Electronic Supplementary Material of this paper). However, as the scan rate increases to 0.4 mV/s, the line is not well fitted. The Randles-Sevcik equation[17] was used to determine ion diffusion coefficients of NCM622. The calculated diffusion coefficients from the anodic and cathodic peaks at 25 and 55 °C are 1.39×10^{-12}, 6.02×10^{-13} and 1.58×10^{-12}, 5.97×10^{-13} cm^2/s, respectively. The results show that the kinetic is diffusion controlled and the ion diffusion did not increase linearly with the elevated temperature.

At elevated high temperature, there may be more phase existed during the electrochemical process[18,19]. In order to further explore the phase change of NCM622 material, we chose *in situ* XRD analysis. Fig.3(A) shows the first-charge profile and corresponding *in situ* XRD patterns of NCM622 at 25 °C. The (003) peak first shifts towards lower angles and then to higher angles, indicating that the c-axis expands first and then contracts during Li extraction, which is in consistent with previous studies[13,20]. The critical Li extraction amount is *ca*. 0.35 per $LiTMO_2$ formula, corresponding to a charge cut off

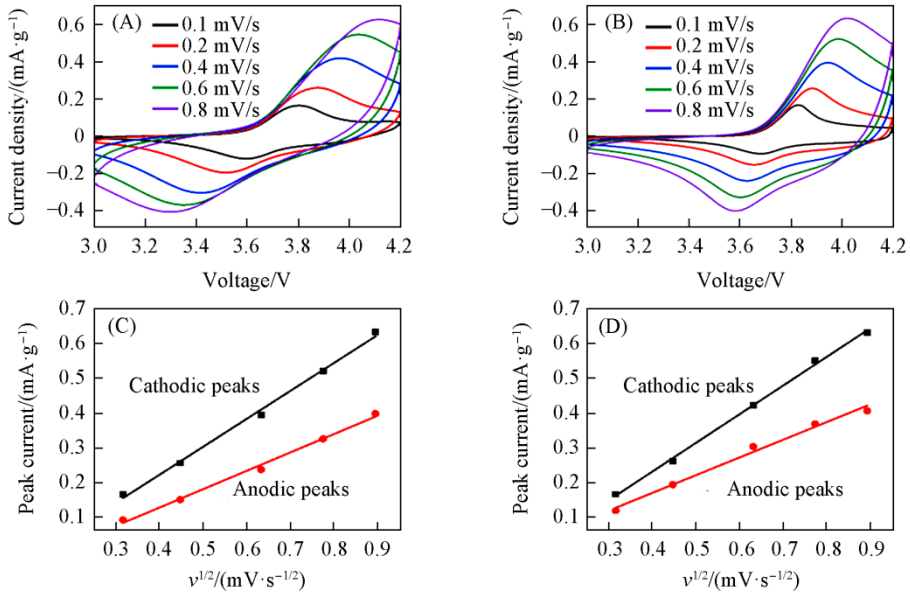

Fig.2 CV curves of 0.1, 0.2, 0.4, 0.6 and 0.8 mV/s at 25(A) and 55 °C(B) and fitted plot of i_p *versus* $v^{1/2}$ at 25(C) and 55 °C(D)

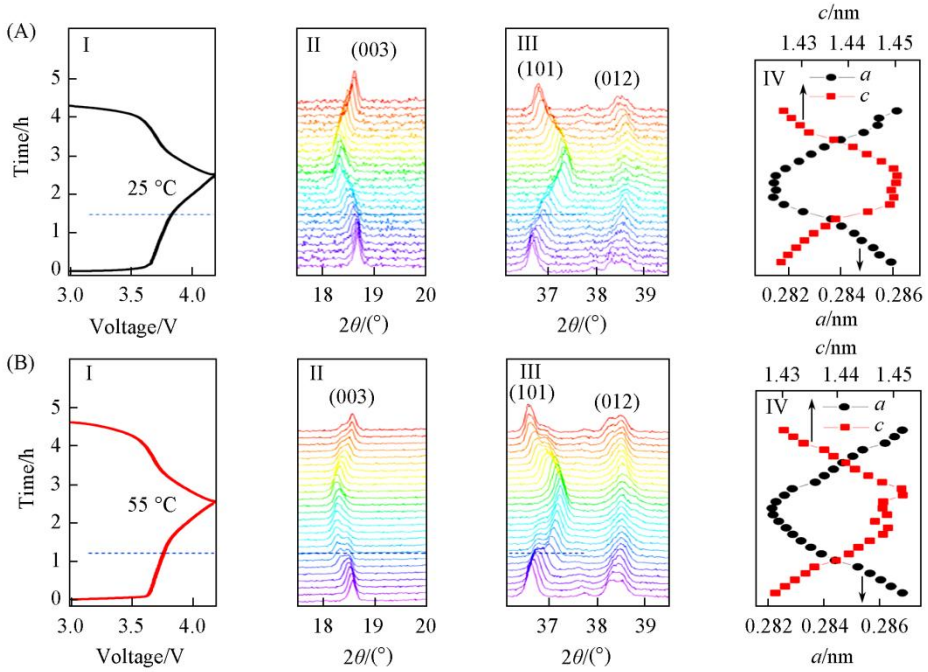

Fig.3 First charge profiles(I), selected *in situ* XRD patterns(II, III) and refined lattice parameters(IV) of NCM622 at 25(A) and 55 °C(B)

voltage of 4.2 V *vs.* Li/Li$^+$. The initial *c*-axis expansion is mainly due to the increased interlayer electrostatic repulsion(mainly oxygen-oxygen repulsion) upon Li$^+$ extraction, and the afterwards significant lattice contraction is attributed to the decreased effective charge of oxygen(increased valance of TMs and thus strength of TM-O bonds)[8]. Being charged to 4.2 V, the (003) peak shifts to *ca*. 18.38°. The rapid expansion of *c*-axis should be coupled with the M-H2 phase transition, as suggested for other Ni-rich NCM[21,22] or $LiNiO_2$, even there is no hint of M-H2 phase transition in CV. The anisotropic lattice contraction upon the M-H2 transition could lead to internal stress and micro-cracks in active particles and thus expose the fresh interface to the electrolytes, which could be the major origin of the capacity fading for Ni-rich NCM[8,9].

Lattice parameters(*a* and *c*) changes during the first charge/discharge process[IV in Fig.3(A)]. Initially, before the M-H2 transition, *a* decreases almost linearly, which indicates an in-plane contraction of *ca*.1.4%, while *c* axis expands *ca*.1.6%. Upon the M-H2 transition, *c* axis expands rapidly, while *a*-axis shrinks slightly and saturates at *ca*. 0.4 Li extraction per $LiTMO_2$. When being charged to 4.2 V, the M-H2 transition only proceeds partially, corresponding to *ca*. 0.5 Li extraction per $LiTMO_2$.

To discern the fading mechanism of NCM622, high-temperature(55 °C) cycling and corresponding *in situ* XRD were carried out[Fig.3(B)]. The high-temperature cycling largely accelerates material fading and facilitates to discover the fading mechanism by *in situ* XRD. At 55 °C, when cycled

between 2.8 V and 4.2 V, peak splitting can be clearly observed for (003) and (101) upon charging. This is distinct from the sequential one-phase and reversible peak shift of NCM622 at 25 °C[II and III in Fig.3(A)]. The peak splitting indicates the formation of the secondary phase, which is further identified to be electrochemically inactive due to its unvaried peak positions(*ca*. 18.30° and 37.05°) upon discharging in this potential range. The fading process(including thermal and electrochemical decompositions) of the active layered phase involves the transition to spinel phase at relatively low delithiated state and further to NiO-like rock-salt structure at high delithiation degrees[23—26]. During the initial several cycles, the secondary phase, appearing at 2θ values of 18.30° and 37.05°, should be assigned to be the spinel phase with a lattice parameter of *a* of *ca*. 0.84132 nm.

The peak intensity and area ratio of the refined $(003)_{layered}$/$(111)_{spinel}$ are *ca*. 2.55 and *ca*. 2.99(Fig.S5, see the Electronic Supplementary Material of this paper). The *in situ* XRD results statistically elucidate the phase evolution processes of NCM622, which are normally derived from spatially resolved technique or theoretical predictions. NCM622 is stably cycled at room temperature, while it is highly unstable at 55 °C.

In addition, widening the working potential range of NCM622 may not fulfil the requirement of safety and energy density at elevated temperature. Coating or doping may be good choice. Also, replacing the commercial graphite with lithium metal is very attractive, while the cell is free from the dendrite[27,28]. Also, when the temperature goes higher, the electrolyte and the lithium poor cathode become more active and more unstable, thus it is hard to determine the malfunctional part. This phenomenon will be more interesting and complex, where more attention should be paied to.

4 Conclusions

Combined with the CV and X-ray diffraction results, the origins of high temperature instability are: (1) the high NCM622/electrolyte reactivity at high temperatures; (2) the NCM622 presents nearly the same diffusion coefficient at 25 and 55 °C; (3) high temperature leads the formation of spinal phase, which is electrochemical inert and the origin of the poor cyclability.

The poor cyclability of NCM622 limits its usage at different temperatures. Thereby, concerns should be given for the commercial implementation of NCM622, especially operating at high temperatures(>55 °C). Solutions will be provided in terms of inhibiting the formation of the spinal phase, which will compromise to the long life of NCM622 at elevated temperature. These findings will give a vivid guidance for the commercialization of layered NCM622, which will realize the development of battery industry.

Electronic Supplementary Material

Supplementary material is available in the online version of this article at http://dx.doi.org/10.1007/s40242-020-0198-8.

References

[1] Chu S., Majumdar A., *Nature*, **2012**, *488*, 294

[2] Mai L. Q., Yan M. Y., Zhao Y. L., *Nature*, **2017**, *546*, 469

[3] Nitta N., Wu, F. X., Lee J. T., Yushin G., *Materials today*, **2015**, *18*, 252

[4] Whittingham M. S., *Chem. Rev.,* **2004**, *104*, 4271

[5] Li W. D., Song B. H., Manthiram A., *Chem. Soc. Rev.*, **2017**, *46*, 3006

[6] Jung R., Metzger M., Maglia F., Stinner C., Gasteiger H. A., *J. Electrochem. Soc.*, **2017**, *164*, A1361

[7] Lim J. M., Hwang T., Kim D., Park M. S., Cho K., Cho M., *Sci. Rep.*, **2017**, *7*, 39669

[8] Yoon C. S., Jun D. W., Myung S. T., Sun Y. K., *ACS Energy Letters*, **2017**, *2*, 1150

[9] Li J., Downie L. E., Ma L., Qiu W. D., Dahn J., *J. Electrochem. Soc.*, **2015**, *162*, A1401

[10] Li W. D., Dolocan A., Oh P., Celio H., Park S., Cho J., Manthiram A., *Nat. Comm.*, **2017**, *8*, 14589

[11] Yan P. F., Zheng J. M., Zhang J. G., Wang C. M., *Nano Lett.*, **2017**, *17*, 3946

[12] Lin F., Markus I. M., Nordlund D., Weng T. C., Asta M. D., Xin H. L., Doeff M. M., *Nat. Comm.*, **2014**, *5*, 3529

[13] Sun H. H., Manthiram A., *Chem. Mater.*, **2017**, *29*, 8486

[14] Chen Z. H., Lu Z. H., Dahn J., *J. Electrochem. Soc.*, **2002**, *149*, A1604

[15] Yan J. H., Liu X. B., Li B. Y., *Rsc Adv.*, **2014**, *4*, 63268

[16] Chen Z., Augustyn V., Jia X. L., Xiao Q. F., Dunn B., Lu Y. F., *ACS Nano*, **2012**, *6*, 4319

[17] Storrow H. A., *Dis. Nerv. Syst.*, **1963**, *24*, 463

[18] Kyeremateng N. A., Vacandio F., Sougrati M. T., Martinez H., Jumas J. C., Knauth P., Djenizian T., *J. Power Sources*, **2013**, *224*, 269

[19] Fabregat-Santiago F., Garcia-Belmonte G., Bisquert J., Bogdanoff P., Zaban A., *J. Electrochem. Soc.*, **2003**, *150*, E293

[20] Li J., Shunmugasundaram R., Doig R., Dahn J., *Chem. Mater.*, **2015**, *28*, 162

[21] Ryu H. H., Park K. J., Yoon C. S., Sun Y. K., *Chem. Mater.*, **2018**, *30*, 1155

[22] Shu J., Ma R., Shao L. Y., Shui M., Wu K. Q., Lao M. M., Wang D. J., Long N. B., Ren Y. L., *J. Power Sources*, **2014**, *245*, 7

[23] Jung S. K., Gwon H., Hong J., Park K. Y., Seo D. H., Kim H., Hyun J., Yang W., Kang K., *Adv. Energy Mater.*, **2014**, *4*, 201300787

[24] Boulineau A., Simonin L., Colin J. F., Bourbon C., Patoux S., *Nano Lett.*, **2013**, *13*, 3857

[25] Liu H., Harris K. J., Jiang M., Wu Y., Goward G. R., Botton G. A., *ACS Nano*, **2018**, *12*, 2708

[26] Bak S. M., Hu E.Y., Zhou Y. N., Yu X. Q., Senanayake S. D., Cho S. J., Kim K. B., Chung K. Y., Yang X. Q., Nam K. W., *ACS Appl. Mater. Interfaces*, **2014,** *6*, 22594

[27] Yue X. Y., Li X. L., Wang W. W., Chen D., Qiu Q. Q., Wang Q. C., Wu X. J., Fu Z. W., Shadike Z., Yang X. Q., Zhou Y. N., *Nano Energy*, **2019**, *60*, 257

[28] Yue X. Y, Wang W. W., Wang Q. C, Meng J. K., Wang X. X., Song Y., Fu Z. W., Wu X. J., Zhou Y. N, *Energy Storage Mater.*, **2019**, *21*, 180